Computers and Geotechnics 61 (2014) 198–208

Contents lists available at ScienceDirect

Computers and Geotechnics

journal homepage: www.elsevier.com/locate/compgeo

Influence of heterogeneity on 3D slope reliability and failure consequence

M.A. Hicks [a,*], J.D. Nuttall [a], J. Chen [b]

[a] Section of Geo-Engineering, Department of Geoscience and Engineering, Faculty of Civil Engineering and Geosciences, Delft University of Technology, P.O. Box 5048, 2600 GA Delft, The Netherlands
[b] State Key Laboratory of Geomechanics and Geotechnical Engineering, Institute of Rock and Soil Mechanics, Chinese Academy of Sciences, Wuhan 430071, PR China

ARTICLE INFO

Article history:
Received 10 December 2013
Received in revised form 25 April 2014
Accepted 11 May 2014

Keywords:
Failure consequence
Finite elements
Heterogeneity
Monte Carlo
Reliability
Risk
Slope stability
Stochastic analysis

ABSTRACT

This paper investigates the influence of heterogeneity of undrained shear strength on the reliability of, and risk posed by, a long slope cut in clay, for different depths of foundation layer. The clay has been idealised as a linear elastic, perfectly plastic Von Mises material and its spatial variability has been modelled using random field theory, whereas slope performance has been computed using a parallel 3D finite element program. The results of Monte Carlo simulations confirm previous findings that three categories of failure mode are possible and that these are significantly influenced by the horizontal scale of fluctuation relative to the slope geometry. In particular, discrete 3D failures are likely for intermediate scales of fluctuation and, in this case, reliability is a function of slope length. The risk posed by potential slides has been quantified in terms of slide volumes and slide lengths, which have been estimated by considering the computed out-of-face displacements. The results show that, for a given horizontal scale of fluctuation relative to the slope geometry, there is a wide range of possible slide volumes and slide geometries. Indeed, the results highlight just how difficult it is to compute a 2D slope failure in a heterogeneous soil. However, they also indicate that, for low probabilities of failure, the volumes of potential slides can be small. This suggests that, for some problems, it may not be necessary to design to very small probabilities of failure, due to the reduced consequence of failure in this case. The techniques developed in this paper will be important in benchmarking simpler 2D and 3D solutions used in design, as there is a need to quantify slide geometries when benchmarking simpler methods based on predefined failure mechanisms.

1. Introduction

This investigation uses random field theory to model the spatial variability of material properties and finite elements to compute geo-structural response. It is the latest in a series of papers investigating the influence of heterogeneity of undrained shear strength (c_u) for a simple slope stability problem. Previously, Paice and Griffiths [1] and Griffiths and Fenton [2,3] considered the influence of isotropic heterogeneity for a 2D slope using a lognormal distribution of c_u and depth-independent statistics. In particular, they demonstrated the importance of accounting for the spatial aspect of variability through implementation of a correlation distance (or scale of fluctuation).

Hicks and Samy [4–7] conducted similar analyses to demonstrate the importance of depth-dependency and anisotropy of the heterogeneity. They assumed a normal distribution of c_u, arguing that this was sufficient for practical ranges (0.1–0.3) of the coefficient of variation of c_u. (This is because the probability of negative values with the normal distribution is then so small, that truncating the normal distribution to ensure positive values has a negligible effect on any analysis [4].) The authors demonstrated a strategy for deriving reliability-based characteristic property values [6] (in line with the requirements of Eurocode 7) and showed that solutions converged at higher degrees of anisotropy of the heterogeneity [4–7]. This implied that the horizontal scale of fluctuation need not always be accurately known, an encouraging result given the difficulty of measuring this quantity in practice. However, the findings were restricted to slope failure in plane strain and the implicit assumption of an infinite scale of fluctuation in the out-of-plane dimension (that is, along the line of the slope).

Spencer and Hicks [8,9], Spencer [10], Hicks et al. [11,12] and Hicks and Spencer [13,14] extended the research to three dimensions. As in Hicks and Samy [4–7], they considered the influence

* Corresponding author. Tel.: +31 (0)15 2787433; fax: +31 (0)15 2783328.
E-mail address: m.a.hicks@tudelft.nl (M.A. Hicks).

http://dx.doi.org/10.1016/j.compgeo.2014.05.004
0266-352X/

of heterogeneity of undrained shear strength on a slope founded on a firm base and identified three categories of failure mode, depending on the horizontal scale of fluctuation relative to the slope geometry. The implications of the research were twofold. Firstly, 2D analysis is only justified for long slopes if the failure mechanism is two-dimensional. For discrete failures, 3D analysis should be considered and slope reliability is then slope length dependent [8–14]. Secondly, for very long slopes (as in flood defence systems), the performance of the whole slope can be reasonably assessed by carrying out a detailed analysis of a shorter "representative" section of the slope and then extrapolating the results to longer sections by simple statistical analysis [14]. In their work, Hicks and Spencer [14] analysed a slope section with a length to height ratio equal to ten, and used the results to successfully predict the reliability of shorter and much longer slopes that had also been analysed in 3D.

This paper continues the work of Hicks and Spencer [14], by considering the range of potential slide volumes and lengths associated with different scales of fluctuation and levels of reliability. For this purpose, a simple automated strategy is devised to estimate the slide volumes and lengths in Monte Carlo simulations. The results provide an increased understanding of the failure mechanisms involved, and of the influence of heterogeneity on slope reliability in general. In particular, they represent a first step towards quantifying the influence of soil heterogeneity on slope reliability and failure consequence within a risk-based framework, by focussing on the uncertainty associated with geometric considerations (e.g. 2D versus 3D and horizontal scale of fluctuation relative to slope dimensions). Note that the general methodology is not restricted to simple parameters such as undrained shear strength, and it has already been used successfully for 2D reliability assessments involving much more complicated (effective stress) models of soil behaviour, such as in analyses of slope liquefaction case histories (Hicks and Onisiphorou [15], Bakhtiari [16]) and rainfall-induced slope failure in unsaturated soils (Arnold and Hicks [17]). However, complex material behaviour and soil model uncertainty are not considered here.

The advantages of confining the current investigation to undrained shear strength are threefold. Firstly, the experience gained with comparable 2D investigations means that the impact of 3D effects can be readily evaluated. Secondly, as moving to 3D leads to a big increase in the required computational effort, the use of a simple soil model means that available computational resources can be focussed on properly modelling the physical size of the problem. Thirdly, the investigation leads directly to assessing the applicability of 3D analytical solutions that are sometimes used in geotechnical design, as these solutions are generally based on simpler models of soil behaviour. For example, attempts have been made by previous researchers (e.g. Vanmarcke [18], Calle [19]) to investigate the probability of failure of long slopes such as dykes and embankments. These techniques are based on simplifications regarding the soil model (e.g. undrained shear strength) and geometry of the failed zone (e.g. a cylindrical failure surface is generally assumed). Therefore, a useful application of the methodology described in this paper is to benchmark (and, where appropriate, improve) simpler 2D and 3D techniques (Li et al. [20], Li and Hicks [21]). To that end, the techniques implemented in this paper relating to failure surface length and geometry are important, because there is a need to quantify the range of slide geometries in benchmarking simpler methods based on predefined failure mechanisms.

The previous investigation by Hicks and Spencer [14] considered a slope directly founded on a firm base; that is, no underlying soil foundation was considered in order to reduce the problem size. In contrast, this paper includes results for different depths of soil foundation layer, to ascertain whether the more severe (bottom) boundary conditions employed previously have any impact on the general conclusions of the investigation. The associated increase in computational requirements, relative to Hicks and Spencer [14], has required the parallelisation of both the finite element code and Monte Carlo process (Nuttall [22]).

2. Methodology

A detailed description of the methodology is given by Hicks and Spencer [14]. In brief, the undrained shear strength (c_u) has been represented by a normal distribution and by the point and spatial statistics of c_u: these are the mean (μ_{c_u}) and standard deviation (σ_{c_u}), which combine to give the coefficient of variation ($V_{c_u} = \sigma_{c_u}/\mu_{c_u}$); and the vertical and horizontal scales of fluctuation (θ_v and θ_h), which are measures of the distance between adjacent zones of similar strength.

The statistics of c_u are used to generate numerical predictions of its spatial variability. For each so-called "random field" of c_u, the first stage is to generate an isotropic standard normal random field of local averages using Local Average Subdivision [23]. This is based on the exponential Gauss Markov covariance function,

$$\beta(\tau_1,\tau_2,\tau_3) = \sigma_{c_u}^2 \exp\left(-\frac{2|\tau_1|}{\theta_1} - \sqrt{\left(\frac{2\tau_2}{\theta_2}\right)^2 + \left(\frac{2\tau_3}{\theta_3}\right)^2}\right) \quad (1)$$

where β is the covariance function, τ is the lag distance, and subscripts 1–3 represent the three coordinate directions (with 1 being the vertical direction). However, as in Hicks and Spencer [14], the random field is initially generated for the scale of fluctuation being equal in all directions (and is often taken to be θ_h). There then follow a series of post-processing stages to arrive at the final field [14]: these are to transform the field to a normal distribution (based on μ_{c_u} and σ_{c_u}) and to distort it to an anisotropic field based on θ_v and θ_h. The final field comprises cubic cells of cross-correlated local averages of c_u, and these values are mapped onto the finite element mesh at the Gauss point level.

Hence, this investigation uses a Monte Carlo approach, in which each realisation is a deterministic finite element analysis of the slope based on a different random field of c_u, a technique often referred to as the Random Finite Element Method [24].

3. Analysis

Fig. 1 shows the problem geometry and finite element mesh details with respect to Cartesian axes x, y and z. A 45° slope, of height $H = 5$ m and length $L = 100$ m, is cut from a clay layer of depth $H + D$, where D is the depth of clay below the slope toe. The front and back faces of the mesh are on rollers preventing movement in the x-direction, and are placed some distance away from the slope toe and crest to minimise each boundary's influence on the failure mechanism; in the case of $D = 0.0$ m the boundary is usually placed 5 m away from the slope crest, whereas, for $D = 3.0$ m, the boundaries are placed 10 m from the slope toe and crest. The bottom of the mesh is fixed, whereas, at the two mesh ends, only vertical displacement is allowed. Griffiths et al. [25] investigated the influence of the mesh ends in computations of 3D slope reliability for a soil exhibiting isotropic heterogeneity, and highlighted the differences between using perfectly smooth and perfectly restrained boundaries. However, the decision herein to adopt an "intermediate" level of restraint for this boundary, by preventing movement in both the x- and y-directions while leaving the z-direction free, is based on Spencer [10], who found that restraining only the y-direction led to a bias towards failure near the mesh ends. This was thought to be due to an increased influence of weaker zones near the mesh ends, arising from the implied

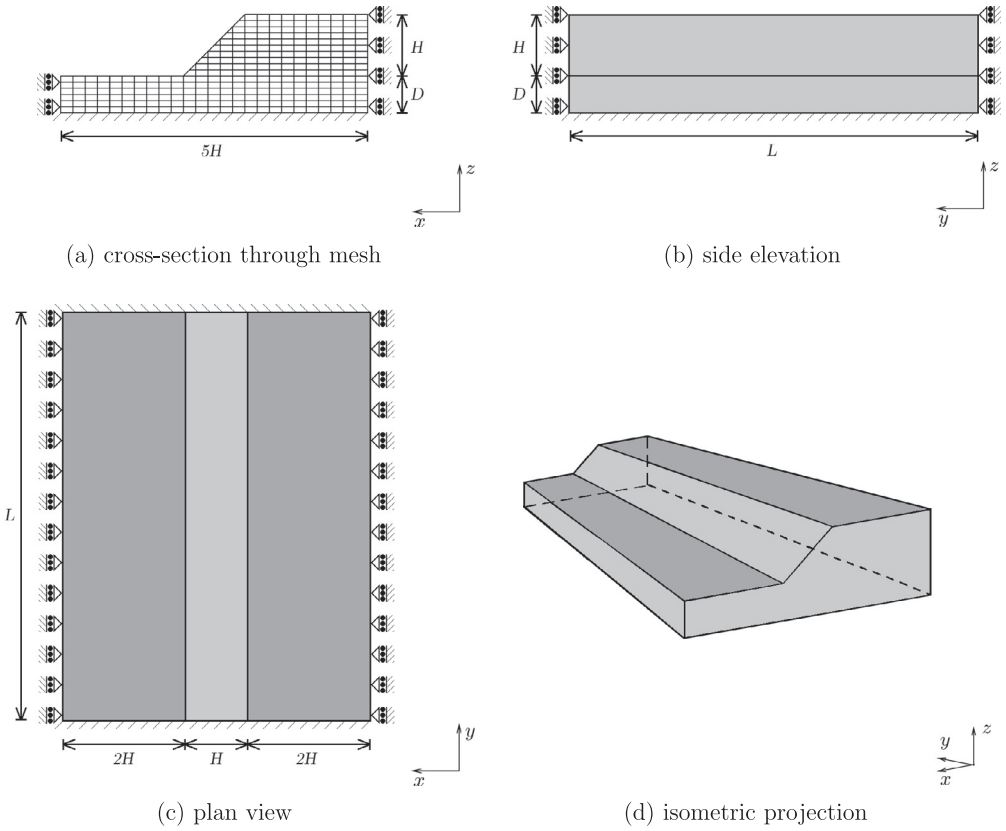

Fig. 1. Slope geometry (not to scale), boundary conditions and finite element mesh details.

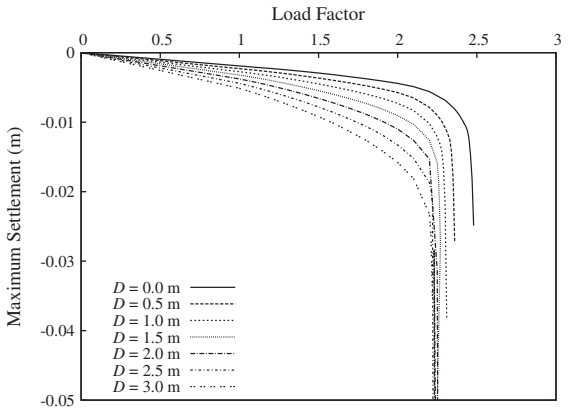

Fig. 2. Influence of foundation layer on load factor versus maximum settlement for a 100 m long homogeneous slope.

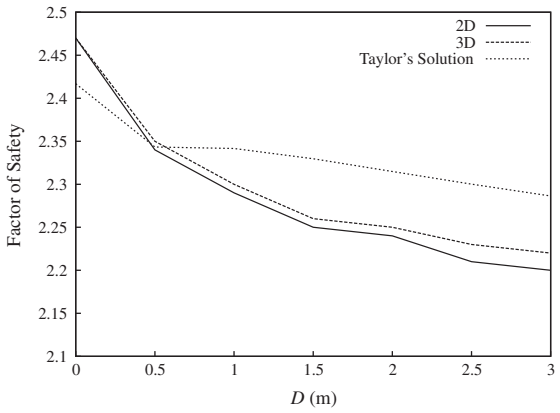

Fig. 3. Influence of foundation layer on factor of safety for a 100 m long homogeneous slope.

symmetry of the random field about this boundary when allowing free movement in the x–z plane. Hicks and Spencer [14] investigated the validity of the boundary conditions, by analysing slopes of different length for the case of $D = 0.0$ m, and produced results supported by probabilistic theory.

The finite element mesh comprises 20-node brick elements. All elements use $2 \times 2 \times 2$ Gaussian integration, and each element is 0.5 m deep and 1.0 m $\times$ 1.0 m in plan, except for those elements that have been distorted to model the slope face. Hence, for $D = 0.0$ m the mesh comprises 8000 elements and for $D = 3.0$ m there are 32,000 elements. In order to assign c_u values to the Gauss points, the random field cell size is 0.25 m (which is half the minimum element dimension). Hence, for assigning values to each finite element there are 32 cubic cells, with each Gauss point value being the average of a group of 4 cells. Further details can be found in Hicks and Spencer [14].

The clay layer has been modelled as linear elastic, perfectly plastic. The elastic component uses a Young's modulus, $E = 100{,}000$ kPa, and Poisson's ratio, $v = 0.3$, whereas the plastic component uses the "internal" Von Mises failure criterion and a spatially varying undrained shear strength (c_u). This is based on a normal distribution and the following set of statistics: depth-independent mean, $\mu_{c_u} = 40$ kPa; coefficient of variation, $V_{c_u} = 0.2$; vertical scale of fluctuation, $\theta_v = H/5 = 1.0$ m; and horizontal scale of fluctuation, $\theta_h = \xi \times \theta_v$, where ξ is the degree of anisotropy of the heterogeneity and is here investigated over the range $0 < \xi < \infty$.

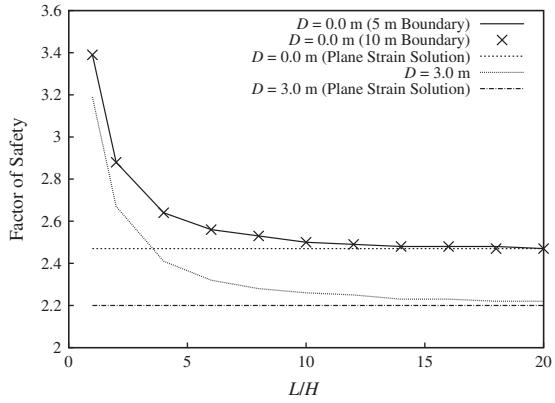

Fig. 4. Influence of slope length on factor of safety of a homogeneous slope.

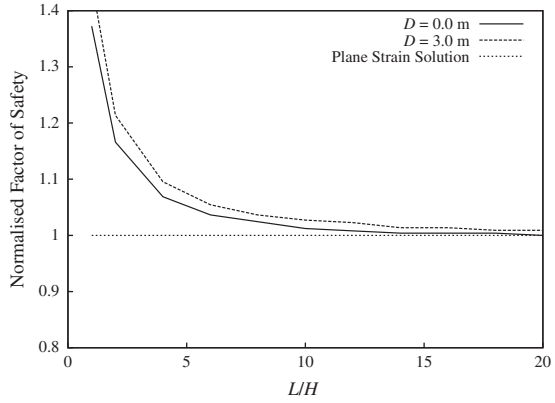

Fig. 5. Influence of slope length on factor of safety relative to plane strain solution.

(a) contours of shear strain invariant

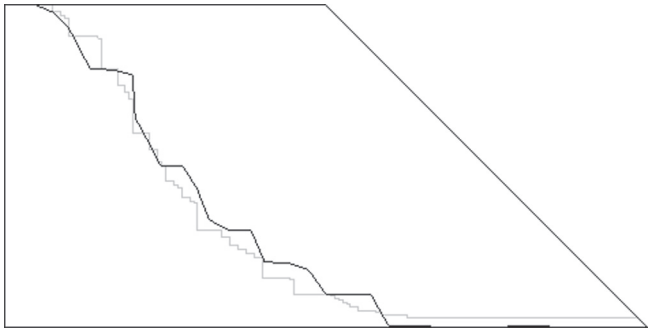

(b) critical failure surface (black) and threshold displacement contour (grey)

Fig. 6. 2D failure mechanism for a homogeneous slope with $D = 0.0$ m.

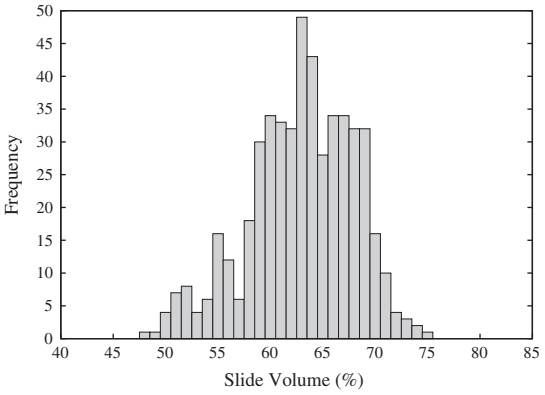

Fig. 7. Slide volume distribution for a 2D heterogeneous slope with $D = 0.0$ m.

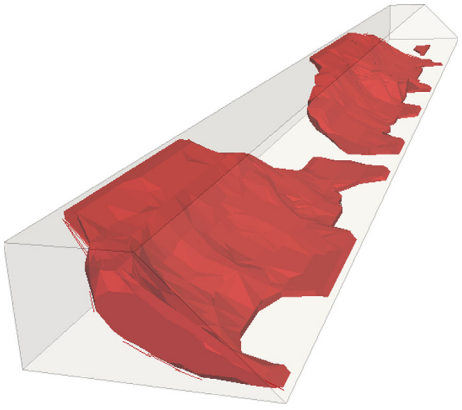

(a) iso-volume of maximum shear strain invariant

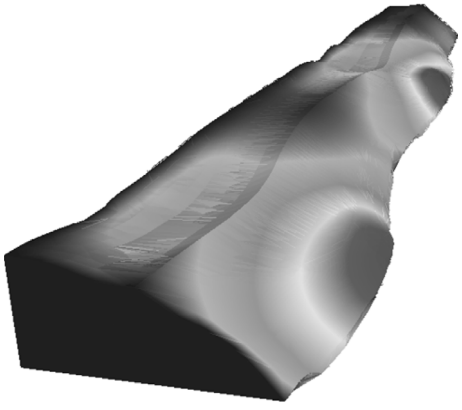

(b) deformed mesh

Fig. 8. Visualisation of multiple failures in a 3D heterogeneous slope with $D = 0.0$ m.

Note that the vertical scale of fluctuation is generally much smaller than the height of a slope and may easily be determined from in situ (e.g. CPT) data [4,5,15], whereas the horizontal scale of fluctuation is generally much larger than the vertical scale of fluctuation and more difficult to quantify [26,27]: hence the reason for keeping θ_v constant and varying θ_h in this investigation.

The slope has been analysed, for each realisation of the random field, by applying gravitational loading to generate the in situ stresses and by finding the conditions necessary for slope failure. For a homogeneous, plane strain slope, of height H and constant undrained shear strength c_u, Taylor's [28] stability number (N_S) is given by

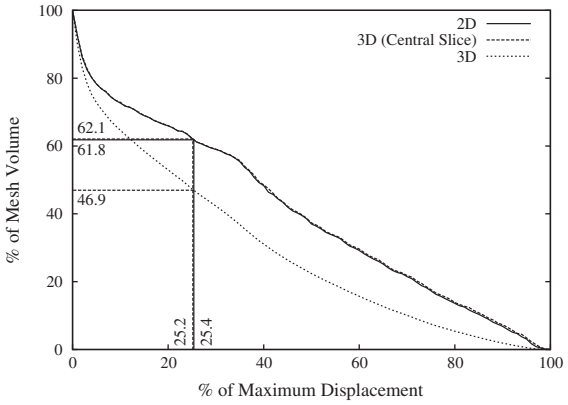

(a) $D = 0.0$ m

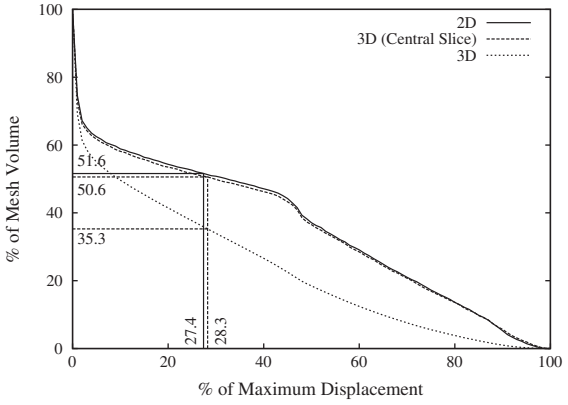

(b) $D = 3.0$ m

Fig. 9. Relationship between percentage of mesh volume and percentage of maximum displacement for a homogeneous slope.

(a) contours of shear strain invariant

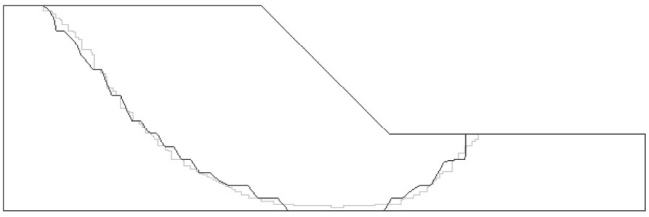

(b) critical failure surface (black) and threshold displacement contour (grey)

Fig. 10. 2D failure mechanism for a homogeneous slope with $D = 3.0$ m.

$$N_S = \frac{c_u}{F\gamma H} \tag{2}$$

where γ is the soil unit weight, F is the factor of safety, and N_S is a function of the slope angle and the ratio D/H [28]. For a heterogeneous slope, the equation may be rewritten as

$$N_S = \frac{\mu_{c_u}}{F\gamma H} \tag{3}$$

where F is now the "global" factor of safety based on the target mean property value μ_{c_u} (and not to be confused with the factor of safety of a potential slide mechanism, which is obviously 1.0 for a slope at the point of failure). Hence, slope failure can be initiated by either decreasing the shear strength profile or increasing the gravitational loading.

Hicks and Spencer [14] followed previous researchers by re-analysing the problem with progressively lower values of undrained shear strength until slope failure occurred. In contrast, this investigation has triggered slope failure by incrementally increasing gravity (while keeping the same shear strength profile). Gravity is increased in incremental steps, with the step size reducing as a function of the maximum incremental nodal displacement as failure is approached, allowing failure to be defined to an accuracy of 0.01 (in terms of the traditional factor of safety) [22]. In this study, slope failure is defined by a load increment failing to converge in 50 equilibrium iterations, using a tangent stiffness approach.

3.1. Monte Carlo simulation

For a given global factor of safety (F), the percentage reliability is given by

$$R = \left(1 - \frac{N_f}{N}\right) \times 100 \tag{4}$$

where N is the total number of realisations and N_f is the number of realisations in which slope failure occurs at or above that value of F. Hicks and Spencer [14] reviewed various strategies for setting up

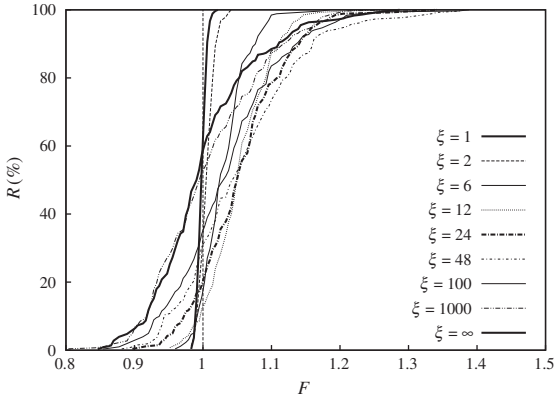

(a) $D = 0.0$ m

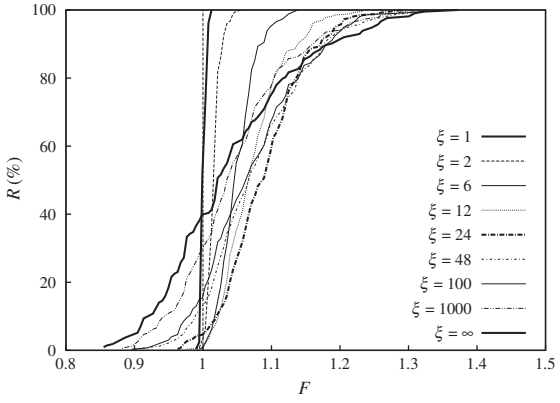

(b) $D = 3.0$ m

Fig. 11. Influence of ξ on reliability versus factor of safety for a 3D slope.

this equation, all of which involved analysing the slope for progressively lower values of c_u (for example, by gradually scaling down the random field values using an increasing strength reduction factor). The value of F at failure (for any realisation) was related to μ_{c_u} at failure through Eq. (3).

For the Monte Carlo simulations in this paper, the mean undrained shear strength for generating the random fields is 40 kPa for each realisation. Hence, for each value of ξ, the reliability distribution has been obtained as follows: firstly, the point and spatial statistics of c_u (i.e. μ_{c_u}, V_{c_u}, θ_v, θ_h) are used to generate N random fields of c_u; secondly, the slope is analysed for each random field in turn, by increasing the gravitational loading until slope failure occurs. The global factor of safety for any realisation is then given by Eq. (3), using μ_{c_u} = 40 kPa, the value of γ at which slope failure occurs and the appropriate value of N_S (which depends on the slope angle (45° in this instance) and D).

3.2. Computing

The current investigation considers the same slope angle, height and length as in Hicks and Spencer [14], and uses the same finite element size. However, the total number of elements is much larger for some analyses (32,000 compared to 8000), due to the consideration of a 3 m deep foundation layer and also to increasing the distance between the back mesh boundary and slope crest to 10 m for the deeper foundation (from the 5 m used previously). Hicks and Spencer [14] used parallel computing to analyse their slope, but, as the mesh was designed to fit on only one computer processor (CPU), only the Monte Carlo simulation was parallelised; that is, the realisations were shared across the processors using a load-balancing technique and, as each realisation was only analysed on one processor, the communication required between processors was minimal. (Moreover, the finite element program used a direct solver and a Tresca failure criterion.)

For this investigation, both the Monte Carlo simulation and finite element program have been parallelised (Nuttall [22]). For the latter, this has been achieved by using an element by element technique: that is, only the element stiffness matrices are required, there is no assembling of a global stiffness matrix, and the equations have been solved using an iterative preconditioned conjugate gradient (PCG) solver. The efficiency of this solver has been facilitated by the use of a Von Mises failure criterion with a suitable return algorithm (Smith and Griffiths [29]). Note that, although the Tresca failure criterion is generally considered to be better than Von Mises for soils, the latter has here been chosen due to the adopted solution algorithm working more robustly and efficiently for a failure surface with no corners.

4. Results

4.1. Deterministic study of homogeneous slopes

Fig. 2 shows the load factor as a function of the maximum mesh settlement, for a homogeneous slope (with c_u = 40 kPa and γ = 20 kN/m^3) and for 0.0 < D < 3.0 m (based on a back boundary 10 m from the slope crest, for all values of D), in which the load factor is the magnitude by which γ is scaled up during an analysis. Each analysis terminates when a load increment fails to converge

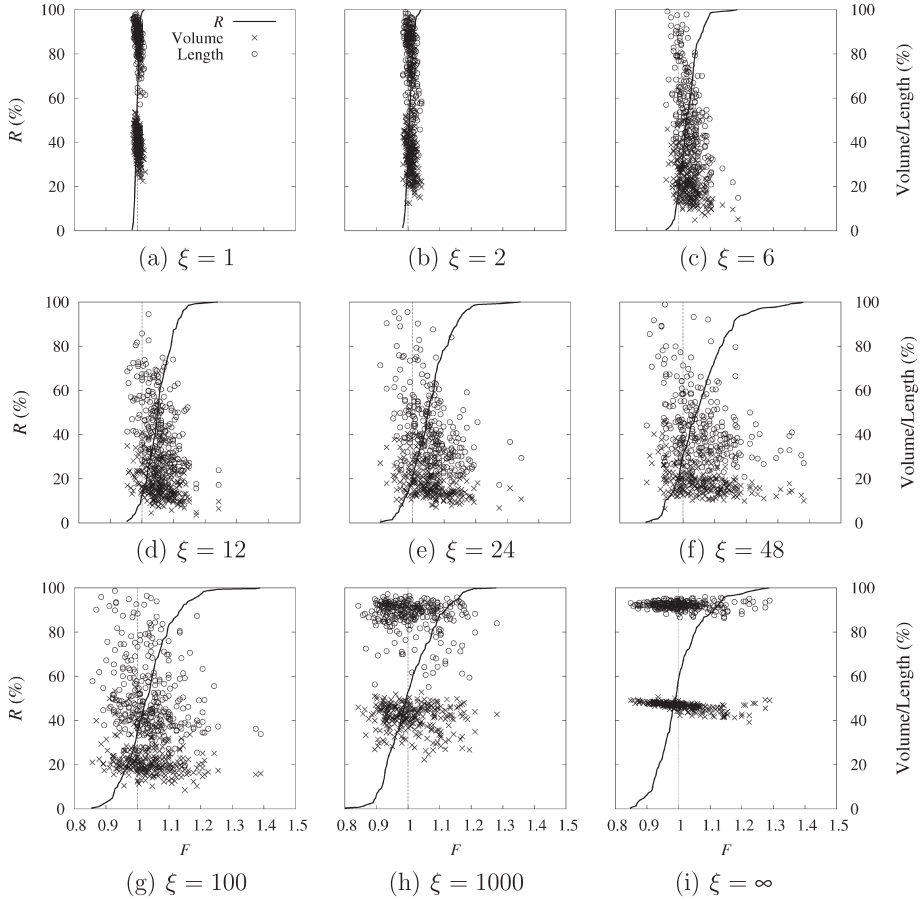

Fig. 12. Influence of ξ on slide volume and length for a 3D slope (D = 0.0 m).

in 50 equilibrium iterations. Fig. 2 shows that this is consistent with the slope failing, as indicated by the settlement increasing very rapidly at constant load. Therefore the curves indicate that a limit of 50 equilibrium iterations has been enough to capture the factor of safety of each slope (corresponding to the load factor at failure).

The factors of safety from Fig. 2 have been re-plotted in Fig. 3 and compare favourably with both Taylor's [28] solution and equivalent 2D plane strain computations. As expected, most of the computed 2D results lie slightly below Taylor's solution due to the use of an internal Von Mises failure criterion; moreover, although the 3D results are stronger than those for 2D due to the different end-boundary conditions, the overall agreement is still very good. The factors of safety for Taylor's solution have been obtained using Eq. (2) and values of N_S ranging from 0.166 to 0.176 (corresponding to the range of D considered). Fig. 3 shows that the end-boundary conditions, whether free or fixed in the x-direction, as modelled by the 2D (plane strain) and 3D analyses respectively, have little influence on the results for a homogeneous slope.

Fig. 4 shows the results of further homogeneous analyses for $D = 0.0$ m and $D = 3.0$ m, for slope lengths in the range, $H < L < 20H$. These show that, for $L/H > 8$, the 3D solution for F is similar to the plane strain solution (see also the findings of Griffiths and Marquez [30]). For $L/H < 8$, the 3D boundary conditions lead to an increase in F and, for $L/H \approx 2$, they impose a failure surface that is approximately spherical. Also shown in this figure are results for $D = 0.0$ m using a mesh in which the far boundary is located only 5 m from the slope crest (as used in Hicks and Spencer [14]). The results are almost identical to the larger mesh for the same value of D, and support the use of the smaller mesh in later Monte Carlo simulations (for $D = 0.0$ m) in order to reduce CPU run-times. Fig. 5 re-plots the same 3D results as a function of the computed plane strain factor of safety for a 2D slope, indicating an increase in F of about 20% for a spherical surface.

4.2. Strategy for estimating slide volumes

In this paper, the consequence of failure has been quantified in terms of the volumes, and lengths, of material associated with potential slides. Hence, this requires an automated procedure for estimating the failure volume and length in each realisation [12,22]. Fig. 6 shows how this may be done for volume in a 2D analysis (in this case, for $D = 0.0$ m). Firstly, contours of shear strain invariant are computed: this is illustrated for a homogeneous slope in Fig. 6(a), in which the darker contours represent larger strains. Next, the critical failure surface is computed by using a ridge-finding technique: this involves selecting an imaginary point in space well above the toe of the slope, and then finding the location at which the shear strain invariant is highest along straight lines radiating out from the point (Fig. 6(b)). The volume of the slide is then easily computed as the area above the critical surface. Note that, in Fig. 6(b), the stepped nature of the critical failure surface is partly a function of the crudeness of the finite element mesh and the effect that this has in back-calculating the discontinuous strain field from the displacement field, and partly due to the (post-processing) smoothing procedure that has been used to obtain a continuous strain field from which the shear strain invariant contours in Fig. 6(a) have been plotted. Although the approximation to the critical failure surface would be smoother for a finer mesh

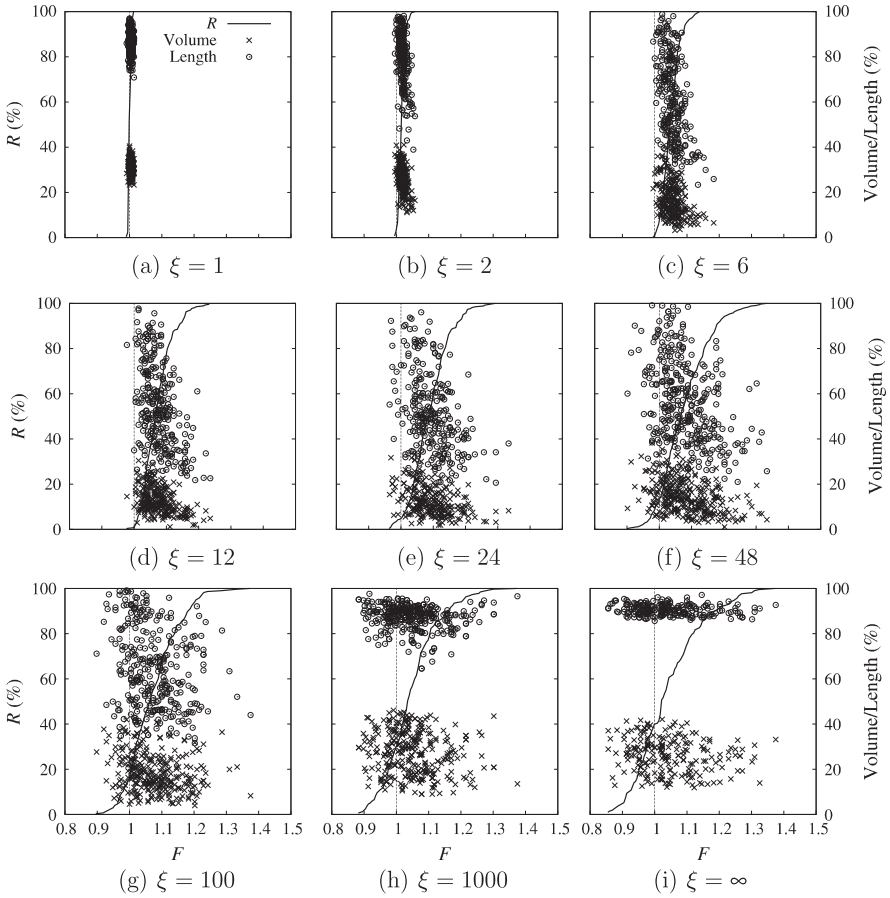

Fig. 13. Influence of ξ on slide volume and length for a 3D slope ($D = 3.0$ m).

discretisation, the relatively crude mesh is still able to give a good result for the failure volume.

Fig. 7 shows typical results from the Monte Carlo simulation of a 2D heterogeneous slope, with $\theta_h = 6.0$ m, in which the slide volume is expressed as a percentage of the total mesh area. Note that all slide depths were around 5 m in this analysis, partly due to the importance of slope height on slope stability for a depth-independent mean strength and relatively low coefficient of variation ($V_{c_u} = 0.2$), and partly due to the steepness of the slope promoting deep sliding (i.e. the slope angle is less than 53°, which is the angle of transition from shallow to deep sliding according to Taylor [28]).

Unfortunately, although the ridge-finding method generally performs well in 2D [12], it was not found to be robust enough for 3D analyses involving soil heterogeneity. Such problems often involve the initiation of multiple and complex rupture zones before the full failure mechanism develops, and this can make the automatic detection of the critical failure surface difficult, especially when multiple and interacting slides are present, as in Fig. 8. Hence, the present investigation uses a simpler approach based on computed displacements in the (out-of-face) x-direction.

Fig. 9 shows the percentage of mesh volume versus percentage of maximum x-displacement, for 2D (plane strain) and 3D homogeneous slopes, as well as for a 2D slice taken through the 3D mesh at $L/2$, for both $D = 0.0$ m (Fig. 9(a)) and $D = 3.0$ m (Fig. 9(b)). That is, for each analysis the maximum nodal x-displacement in the mesh (δ_{max}) is recorded, and then, for a given percentage of that maximum displacement, the volume of the mesh experiencing that displacement or higher is computed. This has been simply approximated as the accumulated volume of all elements, or parts of elements, with an average nodal x-displacement greater than the threshold value. Note that the small ripples in the solution are due to the discrete way in which the volume has been approximated.

Also shown in Fig. 9(a and b) (as horizontal lines) are the percentage volumes obtained by using the above ridge-finding technique to compute the critical failure surface for a 2D slice through the slope. Specifically, for both values of D, two percentage volumes have been computed: the first is based on the shear strain invariant contours produced in the plane strain analysis (as in Fig. 6); whereas the second is based on the shear strain invariant contours for a single-element slice taken through the 3D mesh at $L/2$. Note that both volumes are very similar (for both values of D), indicating that the 3D mesh does deform in a plane strain manner over its central region.

Hence, Fig. 9 can be used to estimate the percentage of the maximum displacement (Δ) that may be used as a threshold to approximate the slide volume: that is, by taking it to be that value which gives the same slide volume as obtained using ridge-finding for a 2D slice taken through the slope at $L/2$. For the plane strain analyses, $\Delta = 25.4\%$ for $D = 0.0$ m and 27.4% for $D = 3.0$ m. Figs. 6 and 10 show that the x-displacement contours corresponding to these displacements are close to the critical failure surfaces obtained using the more rigorous ridge-finding method.

For the 3D analyses, $\Delta = 25.2\%$ for $D = 0.0$ m and 28.3% for $D = 3.0$ m. These threshold displacements have been used to estimate the slide volumes for the 100 m slopes investigated in this paper. Fig. 9(a and b) shows that, based upon these threshold values, the predicted percentage slide volumes for the 3D homogeneous slopes are 46.9% for $D = 0.0$ m and 35.3% for $D = 3.0$ m, which may be compared with the respective percentage volumes of 62.1% and 50.6%, calculated for the 2D slice at $L/2$. The reduction in predicted percentage volume for the whole mesh, with respect to the 2D slice, is partly a function of the boundary conditions restricting failure near the mesh ends. However, an additional (and possibly more significant) factor is that the shear strain gradients are not as high towards the ends of the failed zone, so that the displacements associated with failure in these regions are less than the threshold value estimated at $L/2$. Although this is likely to lead to an underestimation of the true failure volume, the primary goal in the current study is to compare relative failure volumes between realisations. Hence the current formulation is considered sufficient for this purpose, although a more robust method may be desirable in more detailed risk assessments.

A simple procedure has also been adopted for estimating the slide lengths in the following analyses. For each realisation, the slide length is taken to be the integrated length along the slope toe for which the out-of-face displacement is greater than the threshold displacement derived from Fig. 9 (based on the row of elements directly above the slope toe). This simple (but effective) method does not differentiate between the number of slides that occur along the slope length. As for the estimation of failure volume, the intention is merely to provide a consistent way of quantifying and comparing the extent of slope failures.

4.3. Influence of heterogeneity on reliability and slide geometry

Fig. 11(a) shows the influence of ξ, and thereby θ_h ($= \xi \times \theta_v$), on reliability (R) versus global factor of safety (F) for $V_{c_u} = 0.2$ and $\theta_v = 1.0$ m, for $L = 100$ m and $D = 0.0$ m. Each curve is based on multiple (usually 250–300) realisations, with the Monte Carlo simulation being checked to ensure convergence of the output mean and standard deviation. Hicks and Spencer [14] conducted similar analyses for $V_{c_u} = 0.3$ and $\theta_v = 1.0$ m, using a Tresca failure criterion, and identified three categories of failure mode which depended on the magnitude of θ_h relative to the slope geometry. The following general guidelines were proposed [14]:

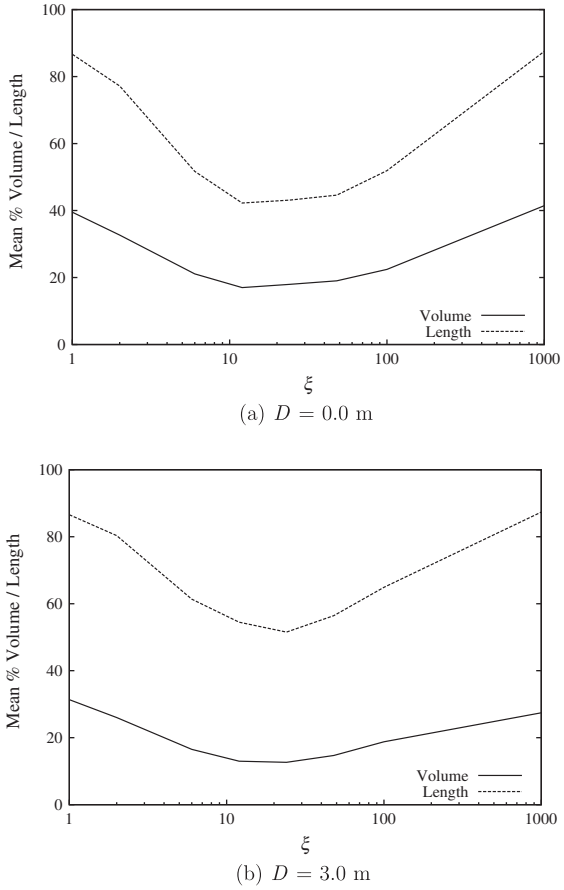

Fig. 14. Influence of ξ on mean slide volume and mean slide length for a 3D slope.

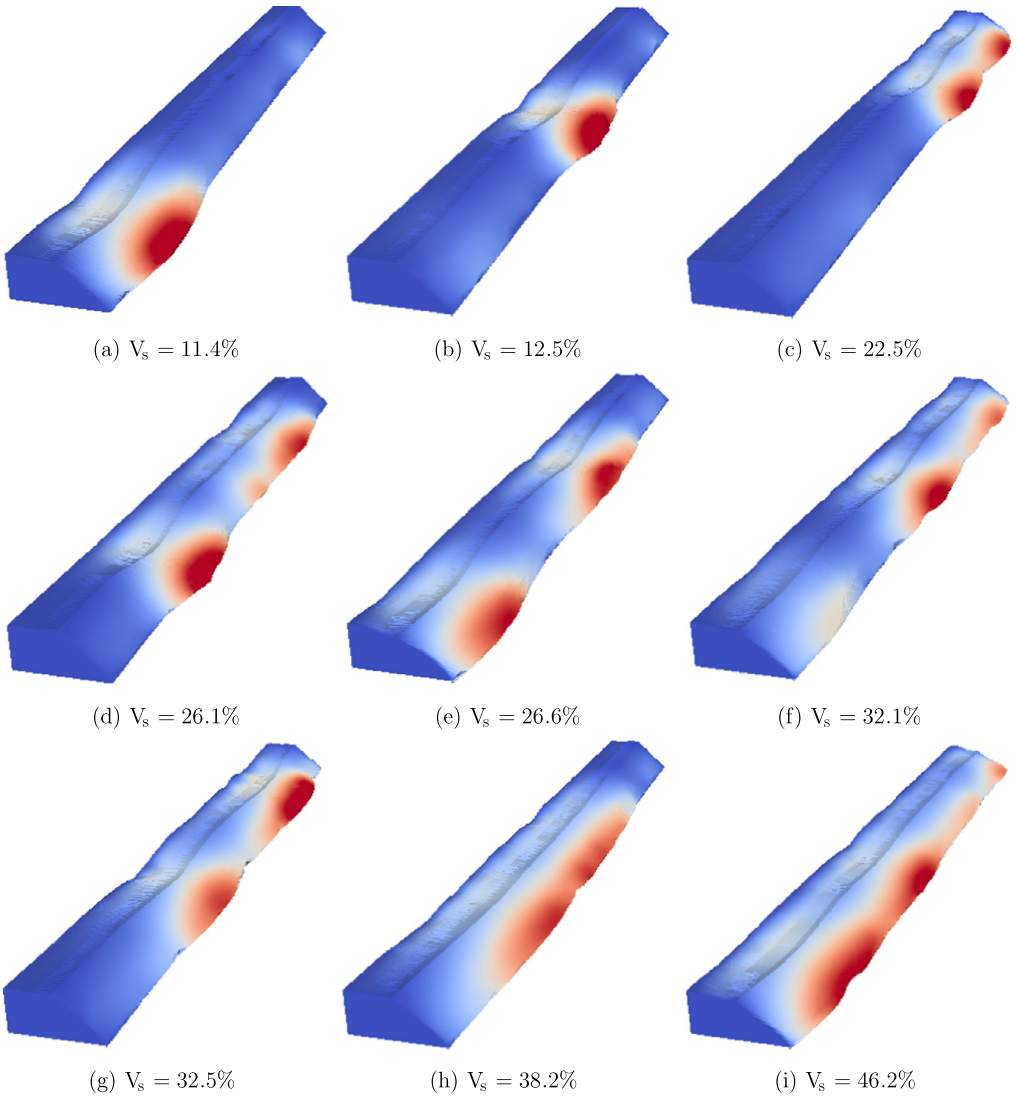

Fig. 15. Example Mode 2 failure mechanisms for $\xi = 6$ (V_s = slide volume, displacement magnification = 75).

- *Mode 1:* for $\theta_h < H$ there is little opportunity for failure to develop through semi-continuous weaker zones. Hence, failure goes through weak and strong zones alike, there is considerable averaging of property values over the failure surface, and the slope fails along its entire length. This case is analogous to a conventional 2D analysis based on μ_{c_u}.
- *Mode 2:* for $H < \theta_h < L/2$ there is a tendency for failure to propagate through semi-continuous weaker zones, leading to discrete (3D) failures and a decrease in reliability as the slope length increases. Hicks and Spencer [14] showed how simple probabilistic theory could be used to predict the reliability of longer slopes based on the detailed stochastic analysis of shorter slopes.
- *Mode 3:* for $\theta_h > L/2$ the mechanism reverts to along the length of the slope. Although it is similar in appearance to Mode 1, it is a fundamentally different mechanism. In this case, failure propagates along weaker layers and there is a wide range of possible solutions that depend on the locations of these layers. The solution for this mode is analogous to a 2D stochastic analysis.

Fig. 11(a) suggests similar findings to Hicks and Spencer [14], as does Fig. 11(b) which shows the results for $D = 3.0$ m. Note the rapid increase in reliability for Mode 1 ($\theta_h < H$; i.e. $\xi < 5$) as the curve passes through $F \approx 1.0$. For Mode 2 ($H < \theta_h < L/2$; i.e. $5 < \xi < 50$), there is a decrease in reliability (for a given F) as θ_h increases, with the weakest result being for $\theta_h \approx L/4$ (i.e. for $\xi \approx 25$). For Mode 3 ($\theta_h > L/2$; i.e. $\xi > 50$), the solution tends towards the plane strain solution as $\xi \to \infty$. The value of θ_h/L at which the dominant failure mode changes from 2 to 3 is rather subjective, but $\theta_h/L \approx 1/2$ seems reasonable, as for larger values it becomes difficult for complete mechanisms to form without some interaction with the mesh ends [14].

However, Figs. 12 and 13 use the methodology developed in Section 4.2 to present a more detailed evaluation of the results, for $D = 0.0$ m and $D = 3.0$ m, respectively. In both figures, parts (a–i) show the individual reliability curves for each value of ξ (and thereby θ_h) and, for each case, the computed slide volumes of all realisations (as a percentage of the total mesh volume) are presented, along with all slide lengths (as a percentage of the total slope length). The significance of the slides in individual realisations can be assessed by comparing with volumes of 46.9% and 35.3%, for $D = 0.0$ m and $D = 3.0$ m respectively, these being the estimated slide volumes for a homogeneous slope based on Fig. 9. In each plot, the slide volumes and lengths are denoted by points relative to the values of F at which slope failure occurred. As can be seen, for each value of θ_h there is a wide range of possible

volumes. However, there is also a clear trend as θ_h increases and this is reinforced by Fig. 14 which highlights the influence of ξ (and thereby θ_h) on mean slide volume and mean slide length.

Focussing first on $D = 0.0$ m, Fig. 12(a) shows the distributions of reliability, slide volume and slide length, for $\theta_h = \theta_v = H/5$ (i.e. $\xi = 1$). All distributions indicate the dominance of Mode 1 failure. That is, R increases rapidly from 0–100% at $F \approx 1.0$, most slide volumes are relatively large ($V_s \approx 30$–50%), and most slide lengths are large ($L_s \approx 70$–100%), indicating failure along most of the slope length. As θ_h increases Mode 2 becomes dominant, as indicated by a greater range of slide volumes and slide lengths, a reduction in mean slide volume and mean slide length, and the possibility of localised slides (for example, as in Fig. 12(c) for $\theta_h = 6\theta_v = 1.2H$ (i.e. $\xi = 6$)). Fig. 15 shows typical failure mechanisms for $\theta_h = 6\theta_v$, which include small and large discrete failures, multiple discrete failures and interacting failures. The computed slide volumes are seen to be consistent with the out-of-face displacement contours, indicating that the method of estimating slide volumes is working well. Fig. 12(a–f) also shows that, as θ_h increases, there is an increasing tendency for smaller slide volumes at larger factors of safety. This suggests that, for some problems, it may not be necessary to design to very small probabilities of failure, due to the volumes of material associated with potential slides then being inconsequential [14]. Indeed, this finding is supported by previous simpler probabilistic studies based on "first crossing" techniques, which investigated the likelihood and expected length of unstable zones as a function of increasing slope length, and thereby provided a theoretical explanation for the expected reduction of slide volumes as the failure probability reduces (e.g. [19,31]).

Fig. 14(a) shows that the mean slide volume and mean slide length reach a minimum when $\theta_h \approx L/4$ (i.e. when $\xi \approx 25$), which also corresponds to the weakest reliability curve (Fig. 11(a)). At first this seems counter-intuitive, since it might be expected that discrete failures become larger as θ_h increases. However, some of the larger volumes and lengths recorded for lower values of θ_h (that are greater than H) are the integrated volume and length arising from multiple failures, whereas, for Mode 2 failures at larger values of θ_h, there is a decreased likelihood of multiple failures due to the constraints imposed by the slope length. In any event, the results in Fig. 14 are only indicative of trends, due to it not differentiating between the number of slope failures in a given realisation.

Figs. 12(e–h) and 14 show that, as θ_h increases beyond $L/4$, the mean slide volume and mean slide length increase, and the tendency for smaller slide volumes at higher F reduces. There is also a gradual transition from Mode 2 to Mode 3 failure as the solution moves towards plane strain at higher values of θ_h. Fig. 11(a) shows the reliability solution has converged to plane strain by the time $\theta_h = 1000.0$ m $= 10L$ (i.e. $\xi = 1000$), whereas Fig. 12(h) shows that most slide volumes are relatively large (30–50%). Note that, although the spread of solutions is still quite large, the slope is found to be at, or near to, failure along the entire length in most instances. Fig. 12(i) shows that, when an infinite horizontal scale of fluctuation is modelled (that is, by using a 1D random field generator), the slide volumes and lengths converge towards those expected for a homogeneous slope.

Figs. 13 and 14(b) show comparable trends in the results for $D = 3.0$ m. The main difference is in the results for the case of $\theta_h = \infty$. As expected, for both $D = 0.0$ m and $D = 3.0$ m, all slope failures extend along nearly the full slope length. However, whereas the slide volumes tend towards the homogenous solution for $D = 0.0$ m, there is still a wide range of solutions for $D = 3.0$ m. The reason for this difference may be explained with reference to the earlier results for homogeneous slopes. Figs. 2 and 3 show that, for the mean c_u considered in this investigation, the factor of safety decreases only slightly as D increases from 1.0 m to 3.0 m. This implies that, whereas the critical slide for a homogeneous slope will extend to the base of the layer, for a heterogeneous slope a wide range of slide depths is likely, regardless of the length of the slide. In contrast, for the $D = 0.0$ m case, the failure mechanism is more strongly influenced by the firm base, because of the slope angle being less than 53°, as previously discussed. Hence, the range of slide volumes is much less in the case of $D = 0.0$ m.

5. Conclusions

The automatic computation of slide volumes for heterogeneous slopes in 3D is difficult, due to the complexity of the underlying failure mechanism. Instead, a simple but effective way of estimating the slide volume based on computed out-of-face displacements has been presented. This is based on defining a threshold displacement, above which the soil volume is deemed to have slipped. The value for this threshold displacement has been estimated by calibrating the out-of-face displacements against the slide volume per metre run at $L/2$ for a homogeneous 3D slope of length L, in which the slide volume may be accurately determined from the shear strain invariant contours using a ridge-finding technique. This gave slide volume estimates that were accurate enough to enable a detailed evaluation of the role of the scale of fluctuation on the performance of heterogeneous slopes.

Previously, Hicks and Spencer [14] analysed a similar slope, but with no foundation layer and with no detailed evaluation of the failure volumes and slide lengths. This investigation has reinforced the previous finding that there are 3 distinct categories of failure mode and that the likelihood of each is a function of the horizontal scale of fluctuation relative to the slope geometry (as defined by the slope height H and length L). Moreover, it has demonstrated the influence of a foundation layer. The new results highlight that, for a given value of the horizontal scale of fluctuation θ_h, there is a wide range of possible slide geometries, and that the previously proposed ranges of θ_h used to identify the occurrence of the three failure modes, while being a reasonable first approximation and a useful aid to understanding the factors influencing slope failure in heterogeneous soils, are not definitive. In particular, Mode 2 (i.e. 3D) failures are possible for almost any value of θ_h and, while they are less likely for $\theta_h < H$, it is apparent that they can occur even for values of θ_h that are large compared to L. Indeed, the results in this paper have highlighted just how difficult it is to compute a 2D slope failure in a heterogeneous soil, even one in which the heterogeneity takes on a "near layered" appearance. Whilst it has been shown that the likelihood of Mode 3 failures increases for $\theta_h > L/2$, it has also been shown that Mode 2 failures remain the prevailing failure mode for horizontal scales of fluctuation up to and even beyond the slope length, especially for slopes that have a foundation layer.

Although this investigation has used a simplified model of soil behaviour, in order to focus on the uncertainty in slope response associated with geometric considerations, in particular relating to soil heterogeneity and slope dimensions, the same methodology can (and will, in due course) be extended to include more advanced aspects of soil behaviour and model uncertainty. In the meantime, the developed techniques will be important in benchmarking simpler 2D and 3D solutions used in design (e.g. Li et al. [20] and Li and Hicks [21]), as there is a need to quantify slide geometries when benchmarking simpler methods based on predefined failure mechanisms.

References

[1] Paice GM, Griffiths DV. Reliability of an undrained clay slope formed from spatially random soil. In: Proceedings of 9th int conf computer methods and advances in geomech, vol. 1, Wuhan; 1997. p. 543–8.
[2] Griffiths DV, Fenton GA. Influence of soil strength spatial variability on the stability of an undrained clay slope by finite elements. In: Slope stability 2000, proceedings of sessions of Geo-Denver 2000, ASCE; 2000. p. 184–93.

[3] Griffiths DV, Fenton GA. Probabilistic slope stability analysis by finite elements. J Geotech Geoenviron Eng, ASCE 2004;130(5):507–18.
[4] Hicks MA, Samy K. Influence of heterogeneity on undrained clay slope stability. Q J Eng Geol Hydrogeol 2002;35(1):41–9.
[5] Hicks MA, Samy K. Influence of anisotropic spatial variability on slope reliability. In: Proceedings of 8th int symp num models in geomech, Rome; 2002. p. 535–9.
[6] Hicks MA, Samy K. Reliability-based characteristic values: a stochastic approach to Eurocode 7. Ground Eng 2002;35(12):30–4.
[7] Hicks MA, Samy K. Stochastic evaluation of heterogeneous slope stability. Italian Geotech J 2004;38:54–66.
[8] Spencer WA, Hicks MA. 3-D stochastic modelling of long soil slopes. In: Proceedings of 14th conf of assoc for computational mechanics in eng, Belfast, UK; 2006. p. 119–22.
[9] Spencer WA, Hicks MA. A 3D finite element study of slope reliability. In: Proceedings of 10th int symp num models in geomech, Rhodes; 2007. p. 539–43.
[10] Spencer WA. Parallel stochastic and finite element modelling of clay slope stability in 3D. PhD thesis, University of Manchester, UK; 2007.
[11] Hicks MA, Nuttall JD, Spencer WA. Stochastic and finite element modelling of 3D heterogeneity in geo-engineering. In: Proceedings of ECCOMAS thematic conf heterogeneous materials with applications in construction and biomedical engineering, Prague, Czech Republic; 2007. p. 236–7.
[12] Hicks MA, Chen J, Spencer WA. Influence of spatial variability on 3D slope failures. In: Proceedings of 6th int conf computer simulation risk analysis and hazard mitigation, Kefalonia; 2008. p. 335–42.
[13] Hicks MA, Spencer WA. 3D finite element modelling of slope reliability. In: Proceedings of 8th WCCM and 5th ECCOMAS, Venice, Italy; 2008.
[14] Hicks MA, Spencer WA. Influence of heterogeneity on the reliability and failure of a long 3D slope. Comput Geotech 2010;37:948–55.
[15] Hicks MA, Onisiphorou C. Stochastic evaluation of static liquefaction in a predominantly dilative sand fill. Géotechnique 2005;55(2):123–33.
[16] Bakhtiari S. Stochastic finite element slope stability analysis. PhD thesis, University of Manchester, UK; 2011.
[17] Arnold P, Hicks MA, A stochastic approach to rainfall-induced slope failure. In: Proceedings of 3rd int symp safety and risk, Munich, Germany; 2011. p. 107–15.
[18] Vanmarcke EH. Reliability of earth slopes. J Geotech Eng Div, ASCE 1977;103(11):1247–65.
[19] Calle EO. Probabilistic analysis of stability of earth slopes. In: Proceedings of 11th int conf soil mech and foundation eng, San Francisco, USA; 1985. p. 809–12.
[20] Li Y, Hicks MA, Nuttall JD. Probabilistic analysis of a benchmark problem for slope stability in 3D. In: Proceedings of 3rd int symp computational geomech, Krakow, Poland; 2013. p. 641–8.
[21] Li Y, Hicks MA. Comparative study of embankment reliability in three dimensions. In: Proceedings of 8th Euro conf num methods in geotech eng, Delft, The Netherlands; 2014 [in press].
[22] Nuttall JD. Parallel implementation and application of the random finite element method. PhD thesis, University of Manchester, UK; 2011.
[23] Fenton GA, Vanmarcke EH. Simulation of random fields via local average subdivision. J Eng Mech, ASCE 1990;116(8):1733–49.
[24] Fenton GA, Griffiths DV. Risk assessment in geotechnical engineering. John Wiley & Sons; 2008.
[25] Griffiths DV, Huang J, Fenton GA. On the reliability of earth slopes in three dimensions. Proc R Soc A 2009;465(2110):3145–64.
[26] Lloret-Cabot M, Hicks MA, van den Eijnden AP. Investigation of the reduction in uncertainty due to soil variability when conditioning a random field using Kriging. Géotech Lett 2012;2(3):123–7.
[27] Lloret-Cabot M, Fenton GA, Hicks MA. On the estimation of the scale of fluctuation in geostatistics. Georisk 2014;8(2):129–40.
[28] Taylor DW. Stability of earth slopes. J Boston Soc Civil Eng 1937;24:197–246.
[29] Smith IM, Griffiths DV. Programming the finite element method. 4th ed. John Wiley & Sons; 2004.
[30] Griffiths DV, Marquez RM. Three-dimensional slope stability analysis by elasto-plastic finite elements. Géotechnique 2007;57(6):537–46.
[31] Vanmarcke EH. On the distribution of the first-passage time for normal stationary random processes. J Appl Mech 1975;42:215–20.